Acta Crystallographica Section B
Structural Science
ISSN 0108-7681

Disordered misfit $[Ca_2CoO_3][CoO_2]_{1.62}$ structure revisited *via* a new intrinsic modulation

Hervé Muguerra,[a]* Dominique Grebille[a] and Françoise Bourée[b]

[a]CRISMAT-ENSICAEN Laboratory, UMR CNRS 6508, 6 Bd Maréchal Juin, F-14050 Caen CEDEX, France, and [b]Laboratoire Léon Brillouin (CEA-CNRS), CEA/Saclay, 91191 Gif-sur-Yvette CEDEX, France

Correspondence e-mail: herve.muguerra@ensicaen.fr

Received 30 October 2007
Accepted 11 January 2008

The structure of the thermoelectric lamellar misfit cobalt oxide $[Ca_2CoO_3][CoO_2]_{1.62}$ was refined again using single-crystal X-ray diffraction data. A new commensurate intrinsic modulation was observed involving a modulation vector orthogonal to the misfit direction (2/3,0,−1/3). The five-dimensional superspace group is $C2/m(1\delta0)(\alpha0\gamma)gm$ and the structure was solved using a commensurate approximation. A new model is given involving an occupation modulation of the split sites of the [CoO] layer. This [CoO] layer can be described by triple chains running along **b**. The residual disorder along **b** can then be explained by the assumption of a local ordering with two types of clusters: CoO_2 and Co_5O_4. A powder neutron diffraction experiment confirmed the ordering evidenced by the single-crystal X-ray diffraction study, but was not sufficient by itself to deal with this double modulated scheme. The new intrinsic modulation is destroyed by partial metal substitutions in the [CoO] layer. The structural modifications of this layer directly influence the physical properties which are related to the electronic structure of the $[CoO_2]$ layers.

1. Introduction

Layered cobalt oxides have been extensively investigated as promising candidates for thermoelectric materials (Terasaki *et al.*, 1997). Indeed they show a large thermoelectric power with a low electrical resistivity and a low thermal conductivity. Recently, the calcium cobalt oxide $[Ca_2CoO_3][CoO_2]_{1.62}$ (CCO) has also been found to exhibit fairly good thermoelectric capacities (Li *et al.*, 1999; Funahashi *et al.*, 2000; Miyazaki *et al.*, 2000). CCO is also fascinating for its original crystal structure. It belongs to the so-called lamellar misfit compounds. It is composed of two monoclinic subsystems exhibiting mutually incommensurate periodicities along **b**, the binary axis direction. The structure can be described as an alternation along **c** of three distorted rock-salt type layers (*RS*; two [CaO] layers sandwiching a central [CoO] layer; first subsystem), and of $[CoO_2]$ layers displaying a distorted CdI_2-type structure (second subsystem).

CCO is a very important compound for understanding and optimizing thermoelectric power coefficients for different reasons. Only three rock-salt layers build the first subsystem of this phase, it is one of the simplest systems of this family. Several structural studies have been published about this compound. It was firstly known, in part, from single-crystal X-ray data refinement on related polytypic phases (Lambert *et al.*, 2001), then from powder diffraction experiments (Miyazaki *et al.*, 2002; Grebille *et al.*, 2004) and more recently from a specific single-crystal X-ray diffraction study (Ling *et al.*, 2007). Other thermoelectric compounds were also structurally

Table 1
Crystal data and structure refinement results of CCO.

Chemical formula	$[Ca_2CoO_3][CoO_2]_{1.62}$	
Formula weight (g mol^{-1})	325.12	
Crystal size (mm)	0.2 × 0.15 × 0.03	
Crystal system	Monoclinic	
Cell parameters (Å)	$a_1 = a_2 = 4.839$ (1)	
	$b_1 = \delta b_2 = 4.553$ (1)	
	$c_1 = c_2 = 10.858$ (3)	
	$\beta = 98.12$ (2)	
$\delta = b_{2,1}/b_{2,2}$	1.6157 (7)	
Superspace group	$C2/m(1\delta0)(\alpha0\gamma)gm$	
Vector modulation	$q_1^* = \frac{13}{8}b_2^*$	
	$q_2^* = \frac{2}{3}a_1^* - \frac{1}{3}c_1^*$	
Z	2	
ρ (g cm^{-3})/μ (mm^{-1})	4.6813/11.163	
Wavelength (Å)	0.70926	
Temperature (K)	300	
Internal consistency factor R_{int} (after absorption correction)		
First subsystem + second subsystem	2.13	
Modulation q_1^*	2.18	
Modulation q_2^*	2.11	
T_{min}/T_{max}		
First subsystem + second subsystem	0.3344/0.7606	
First modulation	0.3356/0.7609	
Second modulation	0.3655/0.7612	
Number of paramaters actually refined	78	
Weighting scheme	$1/\sigma^2$	
No. of unique reflections [with $I \geq 3\sigma(I)$]		Corresponding reliability factor, R/wR
Total	2014	0.0329; 0.0296
Main reflections	1329	0.0259; 0.0265
First subsystem	761	0.0317; 0.0265
Second subsystem	420	0.0222; 0.0268
Common reflections	148	0.0226; 0.0255
Modulation q_1^*	403	0.1190; 0.01405
Modulation q_2^*	737	0.0795; 0.01021

studied: $[Bi_{0.87}Sr_2O_2]_2[CoO_2]_{1.82}$ (Leligny *et al.*, 2000), $[Bi_{0.84}Ca_2O_2]_2[CoO_2]_{1.69}$ (Muguerra *et al.*, 2008) and Na_xCoO_2 (Igarashi *et al.*, 2007). A careful comparison of their common $[CoO_2]$ layers was achieved (Grebille *et al.*, 2007). Rather surprisingly, even with very different crystal symmetries, the structural discrepancies concerning this particular layer are very small and cannot be considered to be significant compared with rather large differences in the thermoelectric power. That is to say that it is also quite important to accurately characterize the *RS* blocks of these phases, which are responsible for the hole doping of the $[CoO_2]$ layer. In the case of CCO, it is now well known that the central [CoO] layer of the *RS* block is characterized by a disorder described by a split-atom model, both for Co and O species. A new structural refinement has been developed for better characterization of this layer, taking into account the observation of a new commensurate modulation perpendicular to the misfit direction. The structure refinement from X-ray single-crystal diffraction data involving both incommensurability in the **b** direction of the misfit, and commensurability in the **a** and **c** directions has proved that this last modulation is related to a partial ordering of the [CoO] layer. From this description, a new model involving two types of clusters is proposed and discussed. The influence of Ga and Fe substitutions on the different layers of CCO will also be described.

2. Experimental

Single crystals were grown by the flux method (Xia *et al.*, 2005). $CaCO_3$ and Co_3O_4 were mixed with a cationic composition of Ca/Co = 2/2.62 for CCO. Fe_2O_3 (or Ga_2O_3) was added in excess in order to obtain Fe- (or Ga-) substituted CCO substituted phases (CCO-Fe or CCO-Ga). The resulting powders were mixed with a $SrCl_2$ flux (weight ratio of 1:2) and heated in a Pt crucible at 1173 K for 12 h. The temperature was lowered to 623 K at a rate of 5 K h^{-1} and then furnace-cooled. The plate-like single crystals have a typical hexagonal surface of 0.02 mm^2 for a thickness of 30 µm. Cationic ratios were obtained by energy-dispersive spectroscopy analysis: Ca/Co = 2/2.54, Ca/Co/Fe = 2/2.32/0.23, Ca/Co/Ga = 2/2.27/0.27.

The single-crystal X-ray diffraction studies were performed at room temperature using Mo $K\alpha$ radiation with a Bruker Kappa CCD diffractometer. For the three compounds, a first cell was determined using reflections with $\theta < 30^\circ$ and is compatible with the monoclinic system: $a_1 = 4.839$ (1), $b_1 = 4.553$ (1), $c_1 = 10.858$ (3) Å, $\beta_1 = 98.12$ (2)°. Other reflections with high intensities were not predicted by this cell, but could be indexed, using a new b_2 parameter, corresponding to the expected misfit structure. A new cell could be refined: $a_2 = a_1$, $b_2 = 2.8178$ (5) Å, $c_2 = c_1$ and $\beta_2 = \beta_1$. Two types of weak satellite reflections are also observed (modulation vectors $\mathbf{q}_1 = (b_1/b_2)\mathbf{b}_2^* + \mathbf{a}_1^*$ and $\mathbf{q}_2 = 2/3\mathbf{a}_1^* - 1/3\mathbf{c}_1^*$). The first set corresponds to the usual satellite reflections resulting from the mutual interaction between the two subsystems of the misfit structure; the second one is only observed in the reciprocal planes corresponding to the first subsystem; that is to say that in a five-indices notation (h, k, l, m, n), n is non-zero only for $m = 0$. No mixed higher-order $(q_1 + q_2)$ or $(q_1 - q_2)$ satellite reflection could be observed. Data collection was performed using φ–ω scans with $0 < \theta < 45^\circ$, with steps of 0.3° per frame and a sample detector distance of 34 mm. Data reduction and integration were performed using the *EVALCCD* software (Duisenberg *et al.*, 2003) in different steps: the main reflections compatible with the first cell (a_1, b_1, c_1, β_1), with the second one (a_2, b_2, c_2, β_2), first-order satellite reflections for vectors $\mathbf{q}_1$ and for $\mathbf{q}_2$. A Lorentz–polarization correction was applied to these data. An analytical absorption correction using the morphology of the crystal based on the measurement of crystal face orientation was performed with the *JANA*2000 software (Petříček & Dusek, 2000). Then they were rescaled using common reflections, merged and averaged using the *JANA*2000 software. For CCO, as it was not possible to deal simultaneously with an incommensurate scheme and a commensurate one, a commensurate approximant was chosen, considering $\delta = b_1/b_2 = 1.6157$ (7) $\simeq$ 13/8. Crystal data are summarized in Table 1.[1] For CCO-Fe and CCO-Ga, the q_2 reflections were too weak and the refinements were performed only with the q_1 modulation.

Neutron diffraction experiments were carried out at the Léon Brillouin laboratory (CEA, Saclay, France) with the

[1] Supplementary data for this paper are available from the IUCr electronic archives (Reference: SN5060). Services for accessing these data are described at the back of the journal.

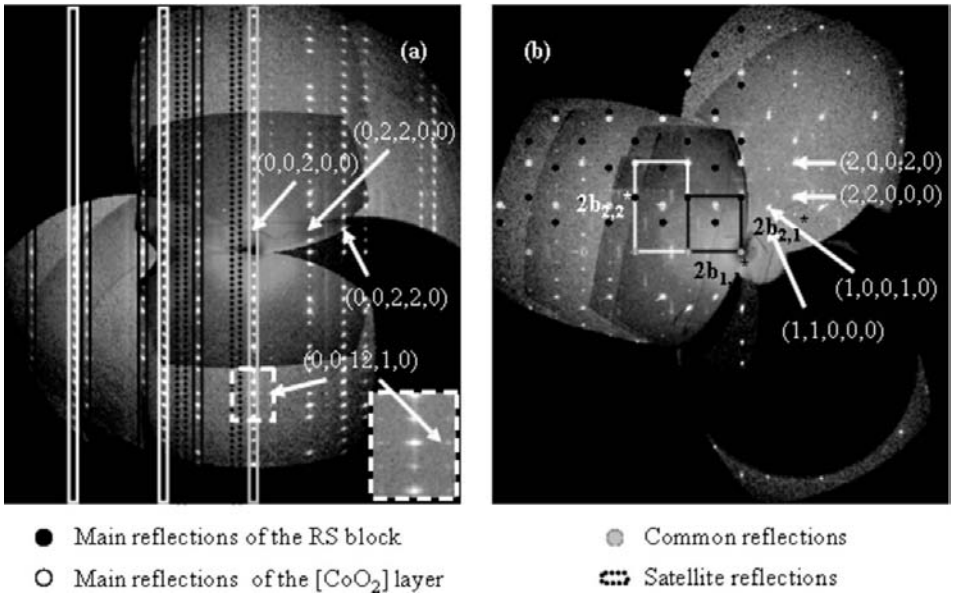

Figure 1
Reconstructed (*a*) (0*kl*) and (*b*) (*hk*0) reciprocal plane of CCO.

high-resolution 3T2 diffractometer using a Ge(335) monochromator and a wavelength of $\lambda = 1.2263$ Å at room temperature. The 2θ range was from 8 to 120° in steps of 0.05°.

3. Structure refinement of CCO

A first analysis of the crystal symmetry of CCO was performed using reconstructed reciprocal planes from the X-ray diffraction data collection. On (0*kl*) and (*hk*0) planes, two types of high-intensity reflections were observed, corresponding to the rock-salt block and the $[CoO_2]$ layer (Fig. 1). These two subsystems share their *a* and *c* parameters, but present different and rationally independent *b* parameters. The aperiodic ratio is $\delta = b_1/b_2 = 1.6157$ (7). The two cells are C-centred. Some weak reflections are also observed on (0*kl*). They result from the intermodulation of the two subsystems and can be explained by the incommensurability along **b**. This modulation can be described by $q_1 = \delta\mathbf{b}_2^* + \mathbf{a}_1^* = 1.6157\ (7)\mathbf{b}_2^* + \mathbf{a}_1^*$, characterized by irrational ($\delta\mathbf{b}_2^*$) and rational ($\mathbf{a}_1^*$) parts.

All these data are in agreement with previous structural models (Grebille *et al.*, 2004; Ling *et al.*, 2007) and with the four-dimensional superspace group $C2/m(1\delta0)s0$ (standard setting). However, in the (*h*0*l*) plane, some weak non-indexed reflections can be observed (Fig. 2). They can be described as satellite reflections using the modulation vector $\mathbf{q}_2 = 2/3\mathbf{a}^* - 1/3\mathbf{c}^*$. In this case the structure presents two independent aperiodicities and cannot be solved in the four-dimensional superspace formalism, but in the five-dimensional one (3D + 2; Yamamoto, 1992). No mixed higher-order satellite reflections could be measured, probably because the intensity of all these first-order satellite reflections are weak and higher-order terms should be weaker still, and also because only the first subsystem will appear to be affected by the second commensurate modulation: no (*h*0*lmn*) satellite reflection could be observed with $m \neq 0$. The superspace group is now $C2/m(1\delta0)(\alpha0\gamma)gm$ with $\delta = 1.6157$ (7), $\alpha = 2/3$ and $\gamma = -1/3$. Eliminating the rational part of the first modulation vector, the previous standard setting can be replaced for the refinement by $X2/m(0\delta0)$-$(\alpha0\gamma)gm$ with a centring vector in five-dimensional space $(\frac{1}{2},\frac{1}{2},0,\frac{1}{2},0)$. For computational reasons, a $3 \times 8 \times 3$ approximant supercell was chosen with $\mathbf{q}_1' = 13/8\mathbf{b}_1^*$ (the intensity integration process in the *JANA* software cannot simultaneously refine incommensurate and commensurate modulations and for this reason, the misfit aperiodicity was approximated to the commensurate value 13/8). A simpler $3 \times 8 \times 1$ cell or a new incommensurate misfit structure with a supercell average structure $3 \times 1 \times 1$ and new centring conditions could be chosen with a new choice of the basic vectors of the monoclinic cell, but we preferred to keep the same stacking and in-plane basic vectors in order to make an easier comparison with previous refinements and to keep the physical and structural significance of these vectors. Structure refinement started from the previous four-dimensional misfit model (Grebille *et al.*, 2004). It included positional first-order

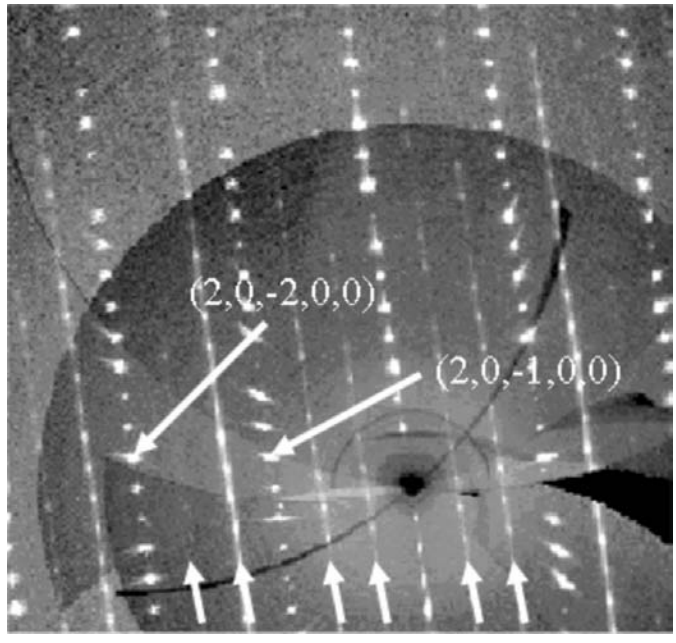

Figure 2
Reconstructed (*h*0*l*) reciprocal plane of CCO. White arrows: q_2 reflection.

Table 2
Atomic positions and modulations functions.

	Wave	Occupancy	x	y	z	U_{iso}
First subsystem						
Ca		1	0.43009 (6)	0†	0.27488 (3)	0.00853 (6)
	sin ($2\pi x_4$)	–	−0.01517 (16)	0†	0.00035 (9)	
	cos ($2\pi x_4$)	–	0†	−0.0012 (4)	0†	
	sin ($2\pi x_5$)	–	0.0012 (2)	0†	0.00050 (10)	
	cos ($2\pi x_5$)	–	0.00060 (2)	0†	0.00308 (10)	
O1		1	0.0527 (2)	0†	0.66413 (10)	0.0110 (2)
	sin ($2\pi x_4$)	–	−0.0027 (7)	0‡	−0.0006 (3)	
	cos ($2\pi x_4$)	–	0†	0.0004 (11)	0†	
	sin ($2\pi x_5$)	–	−0.0011 (7)	0†	0.0005 (3)	
	cos ($2\pi x_5$)	–	−0.0009 (7)	0†	−0.0030 (3)	
Co1*a*		0.279 (5)	0†	0†	0.5	0.0039 (4)
	sin ($2\pi x_4$)	0†	−0.0057 (18)	0‡	0‡	
	cos ($2\pi x_4$)	0†	0†	0†	0†	
	sin ($2\pi x_5$)	0†	−0.011 (3)	0‡	−0.00039 (4)	
	cos ($2\pi x_5$)	−0.177 (10)	0†	0†	0†	
Co1*b*		0.6740 (14)	0.0766 (7)	0.0666 (8)	0.5	0.0044 (3)
	sin ($2\pi x_4$)	0.040 (3)	−0.0050 (9)	−0.0112 (10)	0‡	
	cos ($2\pi x_4$)	0.053 (3)	0.0120 (7)	−0.0276 (9)	0‡	
	sin ($2\pi x_5$)	0.137 (3)	0.0035 (12)	−0.0138 (15)	0‡	
	cos ($2\pi x_5$)	0.008 (3)	0.0167 (15)	−0.0033 (18)	0‡	
O2*a*		0.536 (10)	0.1072 (19)	0.5	0.4996 (4)	0.0099 (14)
	sin ($2\pi x_4$)	0‡	0‡	0†	0‡	
	cos ($2\pi x_4$)	0†	0†	0.029 (3)	0‡	
	sin ($2\pi x_5$)	0.188 (18)	−0.006 (4)	0†	0‡	
	cos ($2\pi x_5$)	0‡	0.012 (5)	0†	0‡	
O2*b*		0.41 (9)	0†	0.421 (2)	0.5	0.0080 (15)
	sin ($2\pi x_4$)	0†	−0.011 (3)	0†	0‡	
	cos ($2\pi x_4$)	0†	0.014 (4)	0†	0†	
	sin ($2\pi x_5$)	0†	0.020 (7)	0†	0‡	
	cos ($2\pi x_5$)	−0.128 (14)	0†	−0.014 (4)	0†	
Second subsystem						
Co2		0.9498 (2)	0.75	0.75	0‡	0.00314 (4)
	sin ($2\pi x_4$)	–	0†	0†	0†	
	cos ($2\pi x_4$)	–	0.00568 (9)	0†	0.00418 (4)	
	sin ($2\pi x_5$)	–	0‡	0†	0‡	
	cos ($2\pi x_5$)	–	0†	0†	0†	
O3		0.9757 (6)	0.38597 (17)	0.75	−0.09328 (7)	0.00587 (15)
	sin ($2\pi x_4$)	–	0†	0‡	0†	
	cos ($2\pi x_4$)	–	0.0067 (3)	0†	0.00294 (16)	
	sin ($2\pi x_5$)	–	0‡	0†	0‡	
	cos ($2\pi x_5$)	–	0‡	0†	0‡	

† Fixed to zero by symmetry. ‡ Fixed to zero as is insignificant.

modulations for all atoms. A split-site disordered model was used for Co and O in the central layer of the *RS* subsystem. A four-dimensional preliminary refinement with only the misfit aperiodicity gave the same results as previously published. Positional first-order parameters were introduced for the second modulation and occupation modulations were also applied to Co and O atoms. Agreement factors and structural parameters are summarized in Tables 1–3.

For the description of the structure, it is important to define u and t. These variables define the different sections of the supercrystal:

$$t = x_4 - q_1'\mathbf{r} \text{ with } \mathbf{q}_1' = \frac{13}{8}\mathbf{b}_1^* \quad (1)$$

$$u = x_5 - \mathbf{q}_2\mathbf{r} \text{ with } \mathbf{q}_2 = \frac{2}{3}\mathbf{a}_1^* - \frac{1}{3}\mathbf{c}_1^*, \quad (2)$$

where x_4 and x_5 are the phases of the harmonic modulation functions related to $\mathbf{q}_1'$ and $\mathbf{q}_2$, respectively, and $\mathbf{r}$ is the corresponding average atomic position in the crystal. Owing to the commensurate character of the $\mathbf{q}_2$ modulation (1/3), only three different sections are physically significant: $u = 0$, $u = 1/3$ and $u = 2/3$ for the Co1*a* atoms of the *RS* block. These three sections approximately correspond to three corresponding x_5 values obtained by the expression

$$u = x_5 - \mathbf{q}_2 \cdot \mathbf{r} = x_5 - \begin{pmatrix} \frac{2}{3} \\ 0 \\ -\frac{1}{3} \end{pmatrix} \begin{pmatrix} 0 \\ 0 \\ \frac{1}{2} \end{pmatrix} = x_5 - \frac{1}{6}. \quad (3)$$

The three values are $x_5 = -\frac{1}{6}$, $x_5 = \frac{1}{6}$ and $x_5 = \frac{1}{2}$.

The same values are also available for the corresponding O2 atoms around $(0,\frac{1}{2},\frac{1}{2})$.

4. Discussion

4.1. CoO_2 layer

All misfit Co oxides share this layer which is at the origin of the thermoelectric properties. It is built with distorted edge-sharing CoO_6 octahedra distributed along a pseudo-hexagonal arrangement. The present refinement involving the second modulation does not significantly modify the configuration of the $[CoO_2]$ layer. Co—O distances are all equivalent (~ 1.90 Å) and are not significantly modified by the modulations (Fig. 3). The octahedra are compressed along the c axis, in relation to a translation of the O

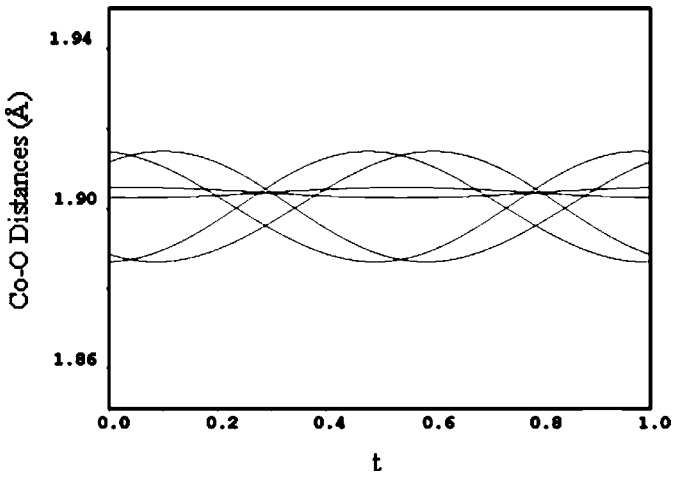

Figure 3
Co—O distances in the CoO_2 layer as a function of t.

Table 3
Refined anisotropic Debye–Waller factors.

	U^{11}	U^{22}	U^{33}	U^{12}	U^{13}	U^{23}
Ca	0.00730 (11)	0.00867 (12)	0.00954 (10)	0†	0.00093 (8)	0†
O1	0.0109 (4)	0.0109 (5)	0.0109 (4)	0†	0.0011 (3)	0†
Co2	0.00218 (6)	0.00284 (7)	0.00444 (7)	0†	0.00057 (5)	0†
O3	0.0047 (2)	0.0053 (3)	0.0076 (3)	0†	0.0013 (2)	0†

† Fixed to zero by symmetry.

layers. The basal plane of the octahedron becomes rectangular, 2.80 × 2.58 Å. The O, Co, O planes are still hexagonal, but the ternary axes through the centre of the triangle-shaped faces are no longer collinear in the distorted octahedron. The thickness of the $[CoO_2]$ layer is about 2 Å, as in $[Bi_{0.87}SrO_2]_2[CoO_2]_{1.82}$ (Leligny *et al.*, 2000) or in $[Bi_{0.84}CaO_2]_2[CoO_2]_{1.69}$ (Muguerra *et al.*, 2008). It is larger than in the Na_xCoO_2 family (1.99 Å in $Na_{0.5}CoO_2$ and 1.96 Å in the $Na_{0.74}CoO_2$; Huang *et al.*, 2004). The Co bond valence can be calculated using Brese & O'Keeffe (1991) bond parameters (+3.5) or it can also be calculated in relation to the Li_xCoO_2 family (Levasseur, 2001; Pollet *et al.*, 2007): +3.36. In both cases, a mixed valence (+3/+4) is found.

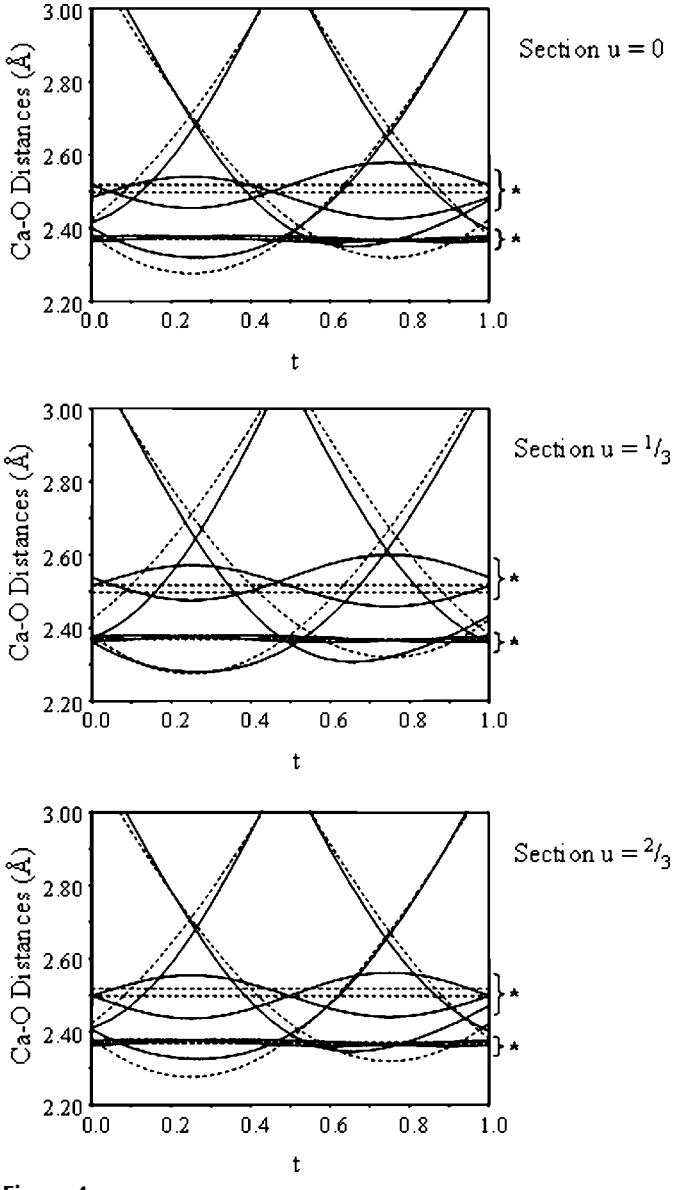

Figure 4
Ca—O interatomic distances with (solid lines) or without (dotted lines) modulations for three sections of the supercrystal. * Ca—O intra-layer distances.

4.2. The rock-salt subsystem

[CaO] is a distorted layer: the Ca sublattice is slightly translated in relation to the O one. Three inequivalent Ca—O distances were found: 2.517 (6), 2.4971 (10) and 2.3691 (3) Å. The modulation scheme of the misfit is related to both the q_1 and q_2 modulations. Owing to the commensurate character of q_2, only three sections are meaningful ($u = 0$, $u = 1/3$ and $u = 2/$

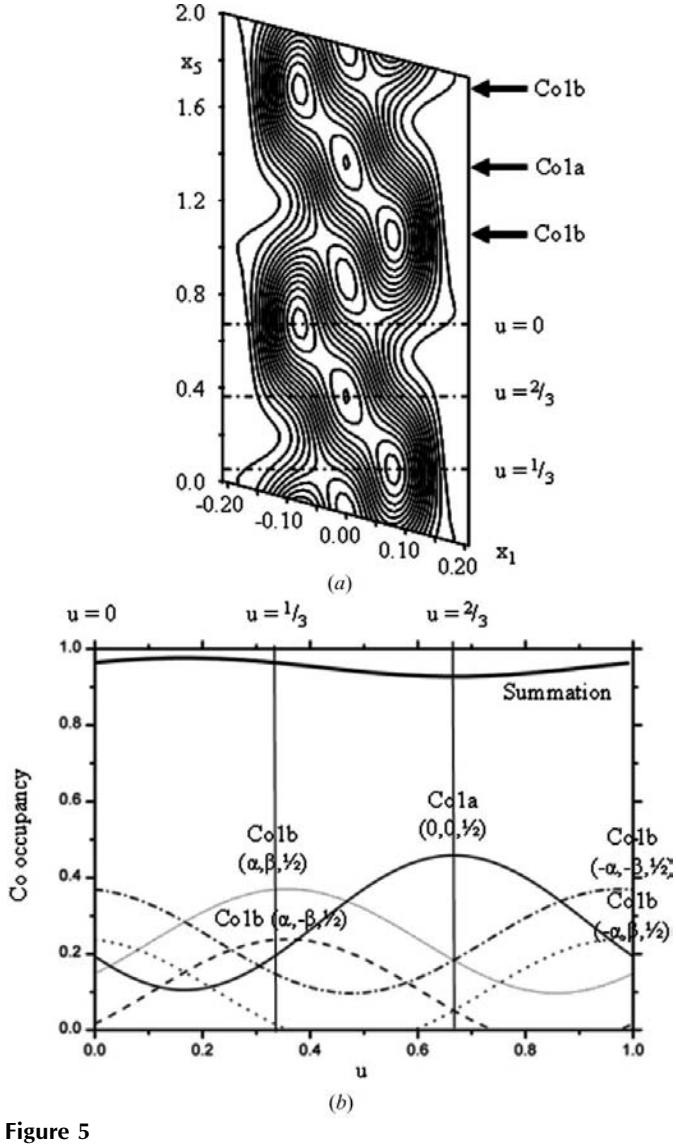

Figure 5
(*a*) Observed Fourier maps of Co atoms and (*b*) variations of Co occupancy within the [CoO] layer as a function of *u*. The different Fourier maps have been summed in x_2 and x_3 directions.

3). The comparison of Ca—O distances with and without modulation for these three sections as a function of t proves that the modulation promotes Ca—O distances around and above 2.3 Å (Fig. 4).

Let us now consider the influence of the threefold modulation within the central [CoO] layer of the *RS* block. The summed observed Fourier maps as a function of x_1 and x_5 show a specific electron-density distribution around the Co and O sites (Fig. 5*a*). It can be described in three sections of high density which represent three different cells in the real crystal. The u = 2/3 section is mainly occupied by the Co1*a* atom, and u = 0 and u = 1/3 by the Co1*b* atom. For the O atoms, the same sections can be found (Fig. 6): u = 0 and u = 1/3 mainly occupied by the O2*a* atom, and u = 2/3, by the O2*b* atom. Observed Fourier maps as a function of x_1 and x_2 can be obtained for each section for the two types of atoms (Fig. 7). All these maps are compatible with the evolution of the Co and O occupation function *versus* u and lead to a common conclusion (Figs. 5*b* and *c*): for u = 0 and u = 1/3, the Co1*b* occupancy is more important than that of Co1*a* for two sites among four. Two equivalent atoms with different x_2 coordinates describe the main part of the density of the Co atom for these sections. The difference between the two sections is the position (< 0 or > 0) of the density as a function of x_1. For u = 2/3, one Co1*a* atom describes the main part of the density. For O atoms, the densities for u = 0 and u = 1/3 are described by one O2*a* atom and for u = 2/3 by two O2*b* atoms with different x_2 coordinates.

The present refinement was achieved using only first-order harmonic modulation functions and this model necessarily introduces smooth partial occupations of the disordered sites. One can imagine another more abrupt and limited model, where one can choose the sites with the larger occupancy as fully occupied, while the other disordered sites are then empty. Then the model should be consistent with a total disappearance of the disorder along x_1, that is to say that both for O and Co species the significantly occupied atomic sites can only be found for one value of x_1, corresponding either to a negative, zero or positive displacement. Concerning the site splitting along x_2, the modulation cannot discriminate between them and the original disorder cannot be eliminated in the case of split sites along this direction (*i.e.* Co1*b* and O2*b*). Summing the occupancies of the different split atomic sites for Co or O positions, rather constant values are obtained (Figs. 5*b* and *c*), close to 0.945 and 0.920, respectively, still suggesting some homogeneously distributed vacancies in this layer.

The alternation of in-phase negative, zero and positive displacements along x_1 for the Co and O atoms results in a triple Co—O chain configuration, running along **b** (Fig. 8*a*). This ordering along x_1 is now compatible with intrachain transverse interatomic Co—O distances around 1.9 Å. Similar BiO double chains were also observed in Bi-based high T_c superconducting Cu oxides or in the misfit Co oxide $[Bi_{0.87}SrO_2]_2[CoO_2]_{1.82}$ (Leligny *et al.*, 2000). However, in these two last cases an incommensurate modulated ordering was also

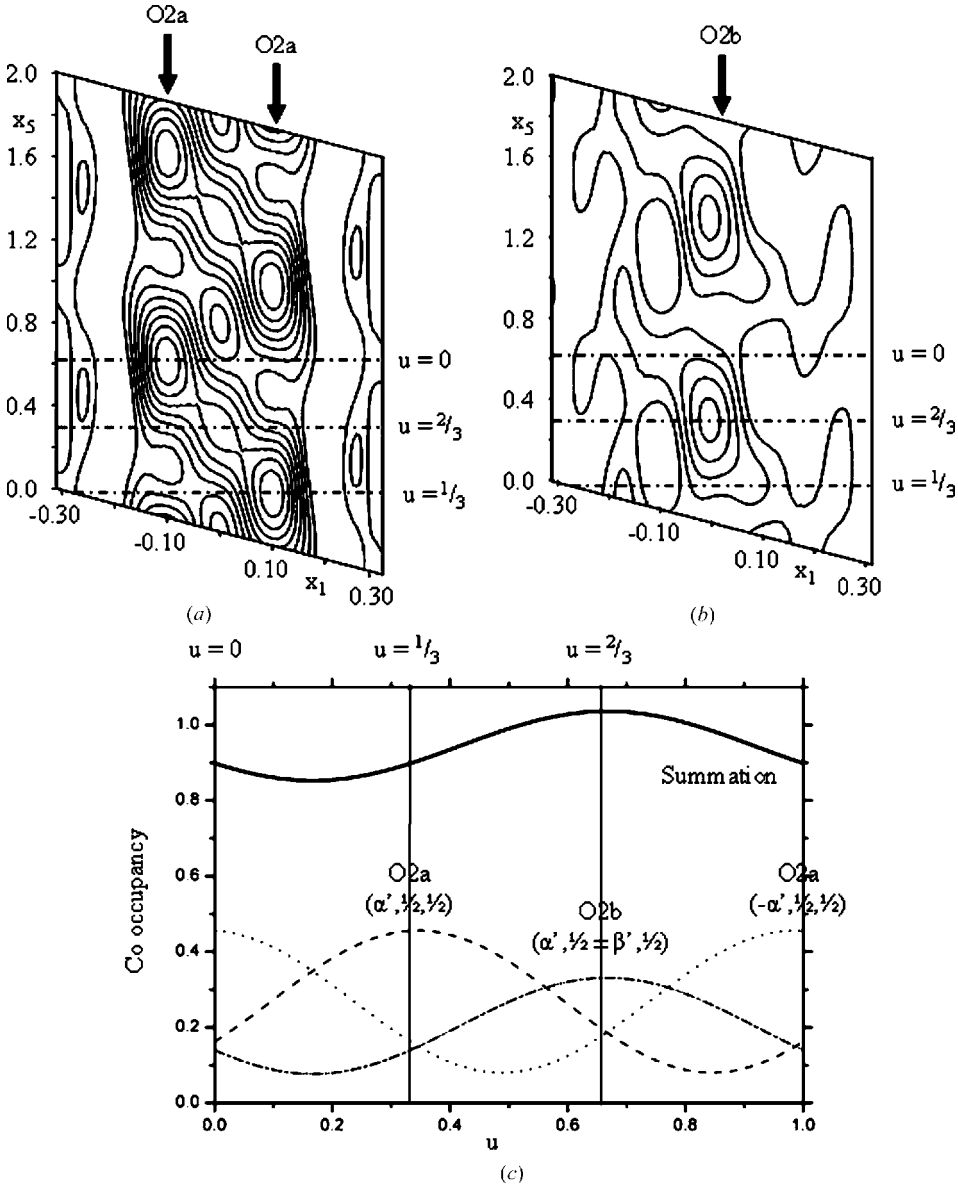

Figure 6
Observed Fourier maps of (*a*) O2*a* and (*b*) O2*b* atoms, and (*c*) variations of O occupancy within the [CoO] layer as a function of u.

performed in the longitudinal direction of the chains, partially raising residual disorders. No evidence for such a modulation can be found here, and it is probably a specific signature related to the presence of bismuth and its electronic lone pair. Nevertheless, in all cases, the tendency to build such chain configurations is probably related to the accommodation of these layers to a cell parameter mismatch with the neighbouring layers. This mismatch is probably the origin of the disorder observed in the present central Co—O layer.

Even if weak diffuse streaks can still be observed along $\mathbf{c}^*$ between satellite reflections, suggesting a partial stacking disorder, the observation of rather well defined satellite reflections proves a rather large coherence length even in this direction, resulting in a general stacking scheme of the triple Co—O layers governed by the z component of the $\mathbf{q}_2$ modulation vector (Fig. 9).

The present structure is very close to the structure of the sulfide compound $[Sr(Fe_{0.77}Nb_{0.23})_{0.5}S_{1.5}]_{1.13}NbS_2$ (Moëlo *et al.*, 1997; Leynaud, 2001; Leynaud *et al.*, 2003), which is characterized by the stacking of a CdI_2-type NbS_2 layer and of a three-layers rocksalt block, also with quite a similar split-atom model in the central $(Fe_xNb_{1-x})S$ layer. On the basis of X ray absorption spectroscopy and transmission electron microscopy measurements, a local structural model involving clusters was proposed. One can also imagine equivalent clusters for a local arrangement of the CoO layer. Then each chain can be considered as a succession of two types of clusters: $[CoO_2]$ and $[Co_5O_4]$ (Fig. 8*b*). Taking into account the neighbouring O atoms of the CaO layer, $[CoO_2]$ has a rather abnormal square coordination and $[Co_5O_4]$ is formed by one octahedron which shares the four edges of its base plane with four tetrahedra. This last cluster is similar to the $[NbFe_4S_4]$ cluster. All of these clusters are compressed along the c axis: Co—O distances are between 1.797 (5) and 1.815 (6) Å. The Co—O distances within the layer are around 2 Å. The $[CoO_2]$ cluster is unusual; it is possible to consider it as a large distorted octahedron which links two $[Co_5O_4]$ clusters within the chain. Within the (**ab**) plane, this octahedron should be composed of two short and two long Co—O distances (1.93 and 2.57 Å). Four Co—O distances are close to 1.9 Å, whereas the Co—O distances in the **b** direction are larger. If only shorter Co—O distances are retained, the square $[CoO_2]$ cluster can be considered.

Therefore, the [CoO] layer can be described as a succession along **a** of chains running along **b**. Each one is built by the alternation along **b** of $[CoO_2]$ and $[Co_5O_4]$ clusters. According to the site occupancy compatible with such a cluster model, one can calculate the average occupation of the Co1*a* and Co1*b*, and the O2*a* and O2*b* sites (0.28/0.72 and 0.42/0.68, respectively). These values are similar to the refined corresponding values, so the model is compatible with the refine-

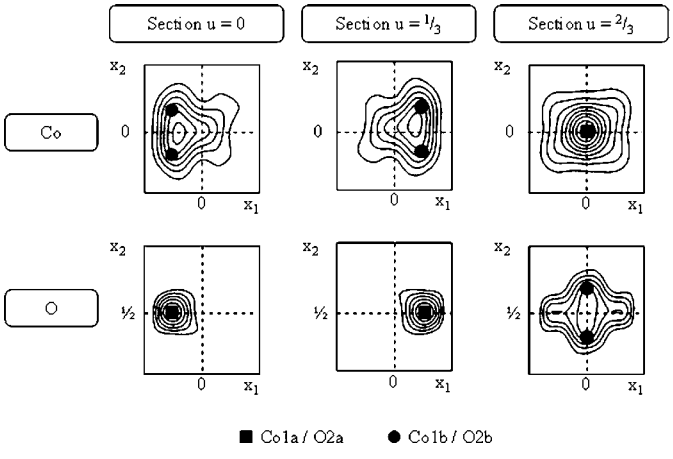

Figure 7
Observed Fourier maps of Co and O atoms within the [CoO] layer for three different sections.

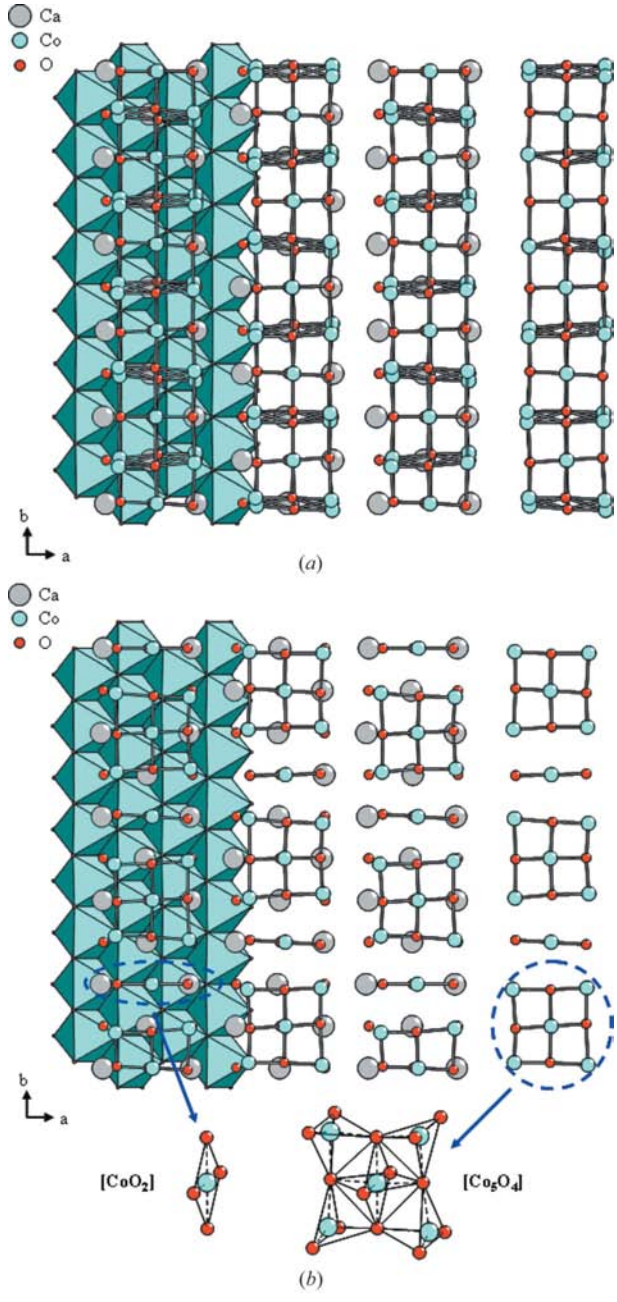

Figure 8
Schematic representation of the [CoO] layer (*a*) by continuous partially disordered chains or (*b*) by cluster chains projected along **c**.

ment. Three different Co valences can be calculated within the [CoO] layer (+2.6 for the squares, +2.3 for the tetrahedra and +3.6 for the octahedra; Brese & O'Keeffe, 1991), which proves the presence of a mixed-valence +2/+3/+4 in this central layer. The average Co valence of the *RS* block is +2.56, which is much lower than +2.8 (Lambert *et al.*, 2001) and +3.14 (Miyazaki *et al.*, 2002) found by other structural studies.

The two types of clusters also interact with the Ca atoms of the [CaO] layers. Three different Ca—O distances can be observed: 2.4467 (15), 2.470 (4) and 2.480 (4) Å. The Ca atoms also interact with the O atoms of the [CoO_2] layer. These Ca—O distances are smaller, between 2.27 and 2.32 Å. Even with various environments imposed by the aperiodicity of the misfit structure, the bond-valence sum for Ca atoms is rather constant between 1.97 and 2.16.

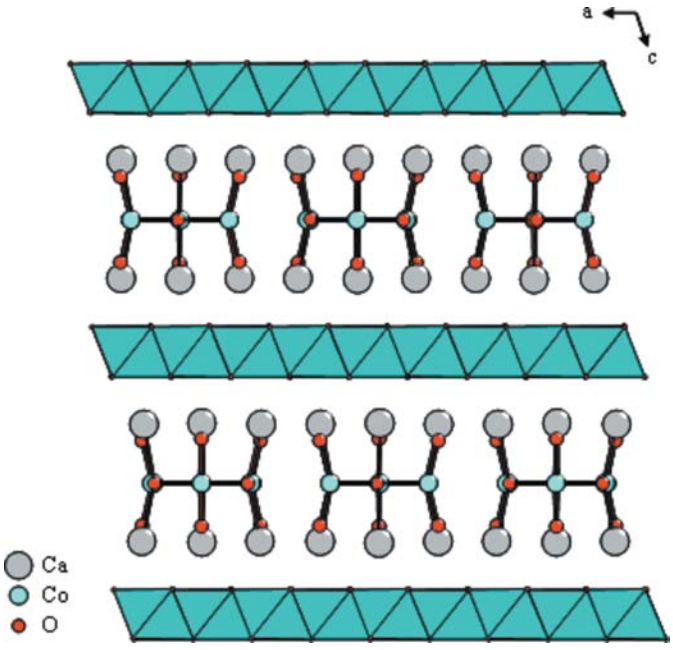

Figure 9
Schematic representation of the structure of CCO along **b**.

In order to confirm this model, in particular for the O atoms, a neutron powder diffraction data set was refined. To account for the line positions, it was now necessary to keep the real incommensurate value of the q_1 vector and, consequently, the q_2 vector was also considered to be incommensurate. In a first step, the planar commensurate modulation was not taken into account and the previous results with the global site atom splitting were still obtained (Grebille *et al.*, 2004). However, the simultaneous refinement of modulation parameters both for the misfit and the intrinsic modulation led to large instabilities and correlations, related to the fact that the refinement process could not find enough weak satellite reflections of both types of modulation in the diffraction pattern. The previous results concerning the misfit structure were then kept constant and only first-order occupation modulation functions were refined for the Co1*a*, Co1*b*, O2*a* and O2*b* atoms, with a phase defined by the $\mathbf{q}_2$ vector. Good agreement factors were obtained: R_p = 0.0322, R_{wp} = 0.0422, R_{Bragg} = 0.0458 (0.0423 and 0.0561 for main and satellite reflections, respectively). Observed Fourier maps were calculated corresponding to the Co, O2*a* and O2*b* atoms (Fig. 10). They are rather similar to those obtained from X ray diffraction data (Figs. 5 and 6), except for a shift in phase for Co1*b* and O2*a* atoms. They confirm the ordering related to the q_2 modulation. One has to keep in mind that this last refinement was largely constrained and, in this case, the Rietveld refinement would not be sufficient and reliable enough without the single-crystal study; this was also the conclusion in the study of the Na_xCuO_2 composite crystal (van Smaalen *et al.*, 2007). Nevertheless, on the basis of the average misfit structure, this new refinement based on neutron diffraction confirms the conclusions drawn from the X-ray refinement concerning the main features of the second modulation.

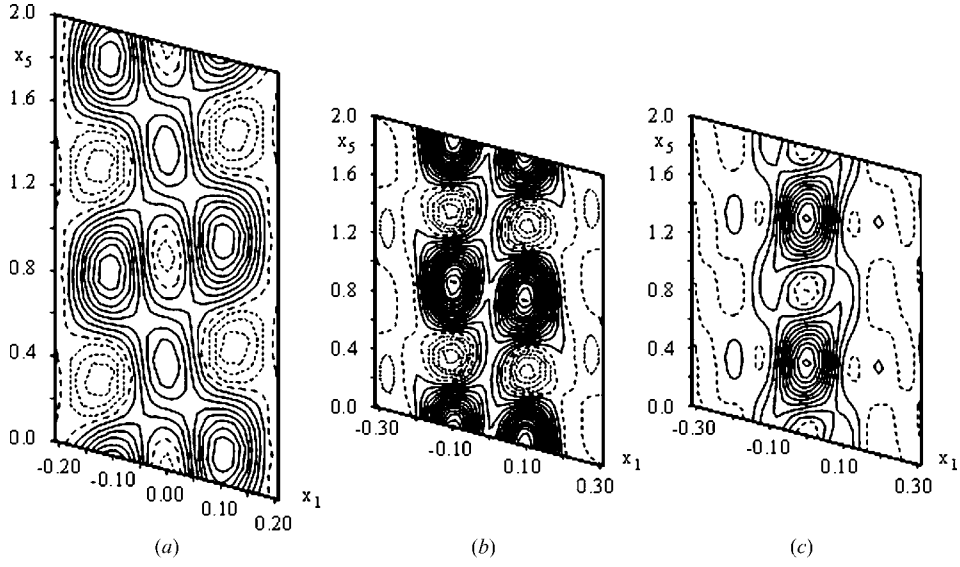

Figure 10
Observed Fourier maps of (*a*) Co atoms, (*b*) O2*a* atoms and (*c*) O2*b* atoms obtained from the powder neutron diffraction data.

4.3. Influence of different substitutions on the [CoO] layer

The partial substitution of other metal atoms (Ga and Fe in our case) for the Co atoms of the central [CoO] layer destroys the commensurate modulation. Structural studies have been made by X-ray diffraction on single-crystal samples for these two phases (Table 4). The two types of substitutions do not affect the global misfit structure; the CCO

Table 4
Crystal data and structure refinement results of CCO-Ga and CCO-Fe.

	CCO-Ga	CCO-Fe
Chemical formula	$Ca_2Co_{2.215}Ga_{0.281}O_{6.119}$	$Ca_2Co_{2.292}Fe_{0.224}O_{6.201}$
Cell parameters (Å)	$a_1 = a_2 = 4.845$ (1)	$a_1 = a_2 = 4.843$ (2)
	$b_1 = \delta b_2 = 4.576$ (1)	$b_1 = \delta b_2 = 4.559$ (5)
	$c_1 = 10.885$ (5)	$c_1 = 10.881$ (4)
	$\beta = 98.08$ (2)	$\beta = 98.07$ (4)
$\delta = b_{2,1}/b_{2,2}$	1.6157 (7)	1.6116 (3)
Superspace group	$C2/m(1\delta0)0s$	$C2/m(1\delta0)0s$
Vector modulation	$q^* = 1.6157\ (7)b_2^* + a_1^*$	$q^* = 1.6116\ (3)b_2^* + a_1^*$
No. of paramaters actually refined	58	58
Weighting scheme	$1/\sigma^2$	$1/\sigma^2$
No. of unique reflections [with $I \geq 3\sigma(I)$]	2484	2473
Main reflections	1177	1170
Reliability factor, R/wR	0.0293/0.0326	0.0314/0.0220
Satellites reflections, first order	1307	1303
Reliability factor, R/wR	0.1683/0.2341	0.1062/0.1145

cell parameters and the symmetry are unchanged. However, q_2 reflections have practically disappeared. A 4*d* structure refinement was performed.

It is interesting to see that these substitutions do not modify the structure of the [CaO] or the [CoO_2] layers, indeed the results of the refinement are the same if the CCO was substituted or not. The CCO structure is very stable, only the versatile [CoO] layer is slightly modified to accept the new type of atom. This phenomenon changes according to the substituting atom. The observed Fourier maps obtained for Co and O atoms of the Ga- and Fe-substituted phases as a function of x_1 and x_2 are different. The usual distribution of their density change (Fig. 11). In the first case the atom splitting along x_2 is stronger. In the second case the opposite phenomenon is observed: the shift along x_2 is reduced and even zero for the O2*b* atom which is no more disordered, but presents a larger anisotropic Debye–Waller factor. The electron density around the O sites of the Fe-substituted phase can be described by only three independent atoms and not four as in CCO or its Ga-substituted phase.

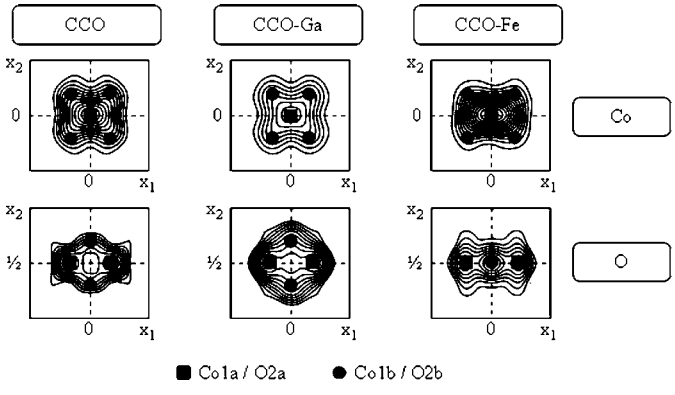

Figure 11
Observed Fourier maps of Co and O atoms within the [CoO] layer for CCO, CCO-Ga and CCO-Fe.

5. Conclusion

A new single-crystal X-ray diffraction investigation of CCO, taking into account a new threefold commensurate planar modulation, allowed us to refine again the misfit structure in the five-dimensional superspace formalism using a $3 \times 8 \times 3$ approximant. The previous structural results are confirmed, but now the central CoO layer of the *RS* block can be described with triple chains running along **b**. A residual disorder is still observed in this misfit direction. From this description, and according to the model previously developed for $[Sr(Fe_{0.77}Nb_{0.23})_{0.5}S_{1.5}]_{1.13}NbS_2$ (Leynaud *et al.*, 2003), one could also propose a configuration with two types of clusters: CoO_2 and Co_5O_4. This confirms different valence states according to the different Co environments. The [CoO] layer is also sensitive to substitutions. For example, Fe or Ga insertion destroys the modulated ordering of the layer and modifies the distribution of the split sites. These chemical and structural changes also modify the physical properties of these phases such as thermopower or electrical conductivity, which are related to the electronic structure in the [CoO_2] layer, so that it appears that in the absence of any significant structural modification in this layer, it is nevertheless very sensitive to the configuration of the sandwiching *RS* block.

The authors thank Hélène Rousselière for technical assistance and X-ray diffraction data collection.

References

Brese, N. E. & O'Keeffe, M. (1991). *Acta Cryst.* B**47**, 192–197.
Duisenberg, A. J. M., Kroon-Batenburg, L. M. J. & Schreurs, A. M. M. (2003). *J. Appl. Cryst.* **36**, 220–229.
Funahashi, R., Matsubara, I., Ikuta, H., Takeuchi, T., Mizutaniand, U. & Sodeoka, S. (2000). *Jpn. J. Appl. Phys.* **39**, L1127–L1129.
Grebille, D., Lambert, S., Bourée, F. & Petříček, V. (2004). *J. Appl. Cryst.* **37**, 823–831.
Grebille, D., Muguerra, H., Pérez, O., Guilmeau, E., Rousselière, H. & Funahashi, R. (2007). *Acta Cryst.* B**63**, 373–383.
Huang, Q., Foo, M. L., Pascal, R. A., Lynn, J. W., Toby, B. H., He, T., Zandbergen, H. W. & Cava, R. J. (2004). *Phys. Rev. B*, **70**, 184110.
Igarashi, D., Miyazaki, Y., Yubuta, K. & Kajitani, T. (2007). *Jpn. J. Appl. Phys.* **46**, 304–310.
Lambert, S., Leligny, H. & Grebille, D. (2001). *J. Solid State Chem.* **160**, 322.
Leligny, H., Grebille, D., Pérez, O., Masset, A. C., Hervieu, M. & Raveau, B. (2000). *Acta Cryst.* B**56**, 173–182.
Levasseur, S. (2001). Thesis. ICMCB University of Bordeaux 1, France.
Leynaud, O. (2001). Thesis. University of Nantes, France.
Leynaud, O., Caldès, M. T., Guillot-Deudon, C., Ouvard, G., Lafont, A. & Meerschaut, E. (2003). *Chem. Mater.* **15**, 3753–3758.
Li, S., Funahashi, R., Matsubara, I., Ueno, K. & Yamada, H. (1999). *J. Mater. Chem.* **9**, 1659–1660.
Ling, C. D., Aivazian, K., Schmid, S. & Jensen, P. (2007). *J. Solid State Chem.* **180**, 1446–1455.
Miyazaki, Y., Kudo, K., Akoshima, M., Ono, Y., Koike, Y. & Kajiitani, T. (2000). *Jpn. J. Appl. Phys.* **39**, L531.

Miyazaki, Y., Onoda, M., Oku, T., Kikuchi, M., Ishii, Y., Ono, Y., Morii, Y. & Kajitani, T. (2002). *J. Phys. Soc. Jpn*, **71**, 491.
Moëlo, Y., Lafond, A., Deudon, C., Coulon, N., Lancin, M. & Meerschaut, A. (1997). *C. R. Acad. Sci. Ser. IIb*, **325**, 287–296.
Muguerra, H., Grebille, D., Guilmeau, E. & Cloots, R. (2008). Accepted for publication.
Petříček, V. & Dusek, M. (2000). *JANA*2000. Institute of Physics, Praha, Czech Republic.
Pollet, M., Doumerc, J. P., Guilmeau, E., Grebille, D., Fagnard, J. F. & Cloots, R. (2007). *J. Appl. Phys.* **101**, 083708.
Smaalen, S. van, Dinnebier, R., Sofin, M. & Jansen, M. (2007). *Acta Cryst.* B**63**, 17–25.
Terasaki, I., Sasago, Y. & Uchinokura, K. (1997). *Phys. Rev. B*, **58**, R12685–R12687.
Xia, C., Sugiyama, J., Itahara, H. & Tani, T. (2005). *J. Cryst. Growth*, **276**, 519–524.
Yamamoto, A. (1992). *Acta Cryst.* A**48**, 476–483.